Proceedings of the
International Conference on Mechanical Engineering 2007
(ICME2007) 29-31 December 2007, Dhaka Bangladesh

ICME2007-KEY-02

ORGANISED STRUCTURES IN WALL TURBULENCE

P. K. Sen[1], S. V. Veeravalli[1], P. W. Carpenter[2] and G. Joshi[1]
[1]Dept. of Applied Mechanics, Indian Institute of Technology Delhi, Hauz Khas, New Delhi -110 016, India

[2]School of Engineering, University of Warwick, Coventry, CV4 7AL, England

ABSTRACT

In our earlier work (Sen & Veeravalli, Sadhana/Proc. Indian Acad. Sci., 1998 and 2000) we have explored the relevance of hydrodynamic stability theory to fully developed turbulent wall flows. Using an extended Orr-Sommerfeld Equation, based on an anisotropic eddy-viscosity model, it was shown that there exists a wide range of unstable wave numbers (wall modes) which mimic some of the key features of turbulent wall flows. Here we present experimental confirmation for the same. As discussed below there is good qualitative and quantitative agreement between theory and experiment. Once the dominant coherent structure is obtained from stability theory, control of turbulence would be the logical next step.

We also present some theoretical work for bypass transition (Klebanoff/K-modes) wherein the receptivity of a laminar boundary layer to a vortex sheet in the free-stream has been studied. The results agree well with the numerical simulations of Fasel (2002). Further to this it is shown that triadic interaction between K-modes, 2D TS waves and 3D TS waves can lead to rapid algebraic growth, which is possibly the cause of bypass transition. A similar mechanism seems to carry over to the inner wall structures in wall turbulence and it is possible that this is the "root cause" for sustenance of turbulence.

Keywords: Organised disturbances, hydrodynamic stability, Klebanoff modes, compliant wall.

1. INTRODUCTION

The relevance of hydrodynamic stability theory to wall bounded turbulent flows was first extensively investigated by Reynolds and co-workers (see for example Hussain & Reynolds, 1972 and Reynolds & Hussain, 1972). Using an eddy viscosity model for the turbulence they derived an Orr-Sommerfeld like equation for turbulent wall flows.

However, they did not find any region of instability in their theoretical work and this was confirmed by their experiments Hussain & Reynolds, 1972.

Sen & Veeravalli (1998 and 2000a) (hereinafter referred to as S&V1 and S&V2 respectively) considered the problem afresh and concluded that the main reason that the previous investigators failed to find any unstable modes was that they used an isotropic eddy viscosity model, which is really not justified close to the wall. The solutions found by S&V1 mimicked some of the key features of wall bounded turbulent flows like the location of the production peak. Further, these modes were found to scale with inner variables and are thus universal. S&V2 also noted that the dominant modes (experimentally) obtained by Hussain & Reynolds (1972), in a turbulent channel, were damped outer modes, because the disturbance frequency was too low.

The aim of the present work is to verify experimentally, the theoretical results of S&V1 and S&V2 and to explore the possibility of controlling turbulence, for example with compliant walls. We also present theoretical work on the receptivity of the boundary layer (laminar) to a vortex sheet in the free stream and discuss its implications to fully turbulent wall flows by considering triadic interactions between K-modes and 2D and 3D TS waves.

2. THEORY

A brief outline of the theory will be presented here. [Details may be seen in Sen & Veeravalli, 1998, 2000a and 2000b.] In the discussion to follow the instantaneous velocity vector u_i and pressure p obey the incompressible Navier-Stokes and continuity

equations. The velocity and pressure fields are usually decomposed in turbulent flows by the well-known Reynolds decomposition; however, here we prefer a triple decomposition as follows:

$$u_i = \overline{u}_i + \tilde{u}_i + u_i'; \quad p = \overline{p} + \tilde{p} + p'. \tag{1}$$

$\overline{u}_i$ and $\overline{p}$ are respectively the mean velocity and pressure, u_i' , p' are the (random) turbulent fluctuations and $\widetilde{u}_i$, $\widetilde{p}$ correspond to an organised (solenoidal) disturbance (with zero mean). The organized disturbance is assumed to be small compared to the turbulent fluctuations. After some algebra, one obtains the dynamic equation for the organised disturbance (reported in S&V1). In deriving the governing equation, the disturbance stream function ψ is assumed to be two dimensional and expressed as

$\psi = \phi(y)e^{i\alpha(x-ct)}$ where α is the spatial wave number, and $c = c_r + ic_i$ is the complex wave speed.

In S&V1 and S&V2 it was shown that the unstable modes obtained are wall modes, which are found to scale perfectly with inner scales. Therefore the governing equation may also be written in terms of inner variables using the friction velocity u_* as the velocity scale and ν / u_* as the length scale (ν is the kinematic viscosity). We denote quantities that are non-dimensionalised by the inner scales with the superscript (+). The details of the non-dimensionalisation and the physical significance of the different terms is given in S&V1; here we present the final equation in inner variables:

$$\begin{aligned} &i\alpha^+[(\bar{U}^+ - c^+)(\phi'' - \alpha^{+2}\phi) - \bar{U}^{+''}\phi] - [\phi'''' - 2\alpha^{+2}\phi'' \\ &+\alpha^{+4}\phi] - [E^+\{\phi'''' - 2\alpha^{+2}\phi'' + \alpha^{+4}\phi\} + 2E^{+'}\{\phi''' \\ &-\alpha^{+2}\phi'\} + E^{+''}\{\phi'' + \alpha^{+2}\phi\}] - \lambda^+E^+[-2i\alpha^+\phi''' \\ &+2i\alpha^{+3}\phi'] - 2i\alpha^+\phi'[\lambda^+E^{+''} + 2\lambda^{+'}E^{+'} + \lambda^{+''}E^+] \\ &= 0 \end{aligned} \tag{2}$$

Equation (2) is in a general form applicable to all wall modes, because the Reynolds number becomes unity in inner variables; only, the eddy viscosity *E,* and the anisotropy function λ, have very weak outer dependence (for details of E and λ see S&V1 and S&V2).

Having formulated the stability equation, we next look at the boundary conditions for channel-flow and boundary layer flow. For a rigid wall, the normal velocity component vanishes at the wall, and this gives the first boundary condition. The second boundary condition is obtained from the 'no-slip' condition. In actuality, it has been shown by Sen et al. (2006) that the outer boundary condition can be the solution of the Rayleigh equation at y > 0.3, for all cases of wall turbulence, where y is scaled by the outer length scale.

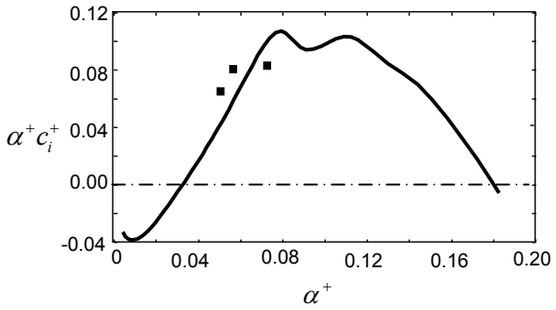

Fig. 1: Growth curve $\alpha^+c_i^+$ versus α^+ (inner variable scaling), Reynolds Number (*R*) for channel flow is 5000. Solid squares are the results from the experiments discussed below.

Figure 1 shows the solution of equation 2. We see that a wide range of unstable wave numbers ($\alpha^+ = 0.03$ to $\alpha^+ = 0.18$) exists. The curve is virtually identical for boundary layer flow and channel flow. It is also insensitive to the location at which the outer boundary condition is applied provided it is larger than one third the boundary layer thickness (or channel height). This agrees very well with the physics of high Reynolds number wall flows. Several other features, like the location of the production peak, agree well with standard measurements.

In case of the compliant wall, the normal velocity components from fluid side and solid side are equated. Further, the resultant velocities for the tangential no-slip conditions at the interface are also equated. Both these conditions are appropriately combined to give the first boundary condition. The second boundary condition is found by equating admittance from the fluid side (*Y*) and to that of solid side (Y_0). Details may be seen in Sen and Arora (1988).

3. EXPERIMENTS

Measurements were made in a 2D channel specially designed for the purpose of this experiment. The half-width of the channel, H, is 0.04m, the spanwise extent, 1.08m and the test section is 12.2m long. The walls (vertical) of the tunnel are made of 12mm thick float glass (each piece 1.22m by 2.44m). A 4.8:1 2D contraction, followed by a small diverging section (to ensure rapid transition) is present upstream of the test section. The organized disturbance is generated by a speaker and introduced into the flow through a slot of 1mm width and 0.15m length, centered in the spanwise direction. A schematic diagram of the set up and the coordinate system used is shown in figure 2.

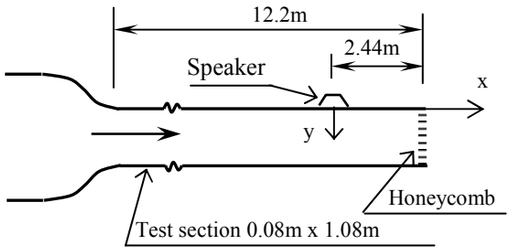

Fig. 2: Schematic diagram of the set-up used for experiments, showing the location of the speaker and the coordinate system in use.

Pressure measurements were made with a Debro micromanometer (resolution 0.01mm) and velocity measurements were made with a boundary layer hot wire probe (5μm dia.) connected to a Dantec 56C17 hot-wire anemometer and 56N20 signal conditioner. The probe was positioned with the help of a travelling telescope fitted with a dial gauge of 1μm resolution. Using this arrangement the distance from the wall could be measured to an accuracy of 0.01mm. Since the wire is at least 0.1mm away from the wall in all the measurements, this accuracy is adequate.

Great care was taken to ensure that the set-up is adequately conditioned for stability work in a turbulent environment. The development length prior to the introduction of the organized disturbance is 244H and the aspect ratio of the test section is 27. These values are large enough to ensure that well upstream of the speaker we have fully developed turbulent flow and that it remains two-dimensional in the central region (greater than 0.4m), throughout the test section (c.f. Hussain & Reynolds 1975). The flow quality in the setup was carefully tested especially in the vicinity of the slot. We note that skin friction measured here agreed to within 0.5% with the data reported in Hussain & Reynolds (1975). The two dimensionality of the disturbance at the exit of the slot and further downstream was also carefully checked and found to be satisfactory.

For the measurements being reported here the average velocity was maintained at approximately 5.3m/s, which corresponds to a Reynolds number of 13,200, based on the half width of the channel. The friction velocity u_* was measured to be 0.28m/s. Phase averages have been obtained over 11,000 cycles at each location.

In keeping with the theory presented above, the organised disturbance $\tilde{u}$, may be expressed as:

$$\tilde{u} = \frac{1}{2}\left\{\hat{u}(y)e^{\imath\alpha(x-ct)} + \text{c.c.}\right\} \qquad (3)$$

where, $\hat{u}(y)$ is the eigenmode. In theoretical work usually α is taken to be real and the complex wave speed c is obtained as an eigen value. Positive c_i thus indicates instability. However, in experiments, it is the circular frequency $\beta = \alpha c$ that is real and both α and c are complex. Thus in the experiments the spatial growth rate is given by $-\alpha_i$ and the equivalent temporal growth rate is $-\alpha_i c_{gr}$, where, c_{gr} is the group velocity. However, our calculations show that the wave speed is nearly constant over the range of wave numbers of interest, thus, the group velocity is the same as the phase velocity. Hence, the equivalent temporal growth rate in the experiments may be estimated as $-\alpha_i c_r$.

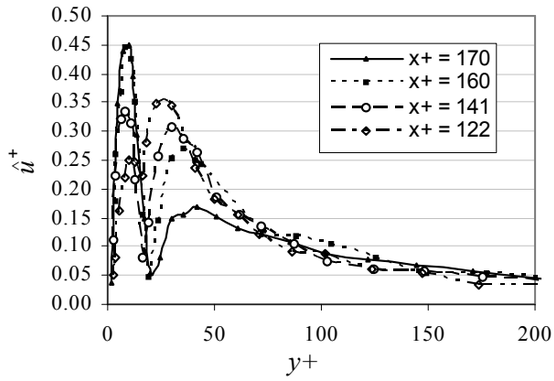

Fig. 3: Evolution of the normalized eigenmode $\hat{u}^+$, with distance from the slot. The speaker frequency has been set at 300Hz which corresponds to $\beta^+ = 0.385$. The distance from the slot has been specified in wall units in the legend and it corresponds to a variation from 7mm to 10mm.

Figure 3 shows the evolution of the eigenmode $\hat{u}^+$, non-dimensionalised by inner variables. The speaker was excited at a frequency of 300Hz, which corresponds to $\beta^+ = 0.385$. This value was chosen so as to be close to the most unstable wave according to S&V2. The four locations (x = 7mm, 8mm, 9mm and 10mm) shown here, correspond to an x^+ range of approximately 120-170. The data clearly show that the inner peak grows rapidly between x=7mm and x=9mm after which it appears to saturate. Beyond x=10mm, the eigen mode is found to decay (results not shown here), with the inner peak moving outwards.

The eigen mode (especially at x=10mm) matches the calculations of S&V1 and S&V2 quite well both qualitatively and quantitatively. Typical results of the calculations for channel flow are shown in Figure 4, wherein, $\hat{u}^+$ and $\hat{v}^+$ are reported for a wave number close to that of the experiments.

The vertical scale in Figure 4 is arbitrary and has been chosen to permit easy comparison with the experimental results. The peaks in the calculations are a little closer to the wall as compared to the experimental peaks, however, the ratio of the two peaks is very close to that observed in the experiment at x = 10mm.

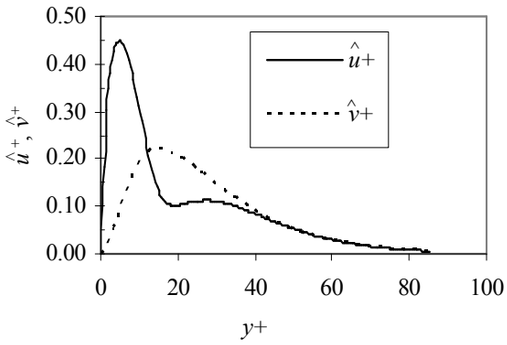

Fig. 4: Calculated eigenmodes $\hat{u}^+$ and $\hat{v}^+$, for channel flow at a Reynolds number of 5000. $\alpha^+ = 0.057$; $c_r^+ = 5.39$ and $c_i^+ = 1.05$.

The fact that the secondary (outer) peak reduces as we proceed from x=7mm to x=10mm, is probably indicative of a competition between two modes initially.

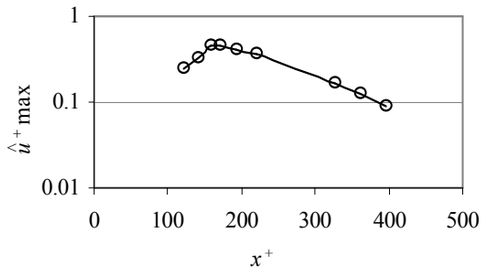

Fig. 5: Evolution of the inner peak of $\hat{u}^+$ in the channel flow experiment. The disturbance frequency was set at 300Hz.

Figure 5 shows the evolution of the inner peak in the experiments. One observes a period of rapid growth followed by a somewhat slower decay. From the figure both the growth and decay appear to be exponential. From the growth of the inner peak and the phase of the eigen mode one can estimate α and c as:

$\alpha_i^+ = -0.015$; $\alpha_r^+ = 0.067$; $c_i^+ = 1.24$; and $c_r^+ = 5.5$

If this is compared with the results of S&V2 it is found that the data here falls almost on the $\alpha^+ c_i^+$ vs. α^+ curve. This can be seen in figure 1 wherein the above datum and those from two other runs with different disturbance frequencies are shown as solid squares. Such a remarkable match compels us to conclude that the growth phase is indeed exponential and according to the theory presented in S&V1 and S&V2, and that this growth is followed by non-linear saturation and decay. However, when the measurements were repeated with a smaller disturbance amplitude (results not shown here) the point of saturation was observed to be the approximately the same, thereby ruling out the conjecture of non-linear saturation. This indicates that the phenomenon is more complex than it appears at first glance. More detailed investigations are underway.

For completeness we also include spectral measurements here. Figure 6a shows the compensated one-dimensional spectra $f F_{11}(f)$ (where f is the frequency) obtained at different distances away from the wall for a downstream distance of 10mm ($x^+ = 174$) and a disturbance frequency of 300Hz. The organized disturbance appears as a clearly distinguishable spike, at the disturbance frequency, in these spectra. We note that as expected the spike lies on the energy containing range. The variation of the magnitude of the spike is consistent with the egienfunction plot shown in Figure 3.

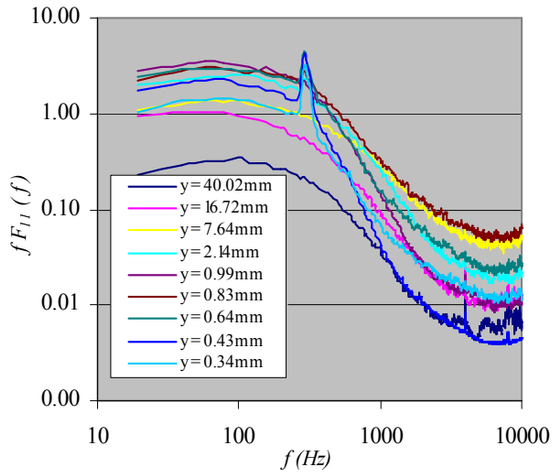

Fig. 6a: Evolution of the peak in the spectrum at different distances from the wall.

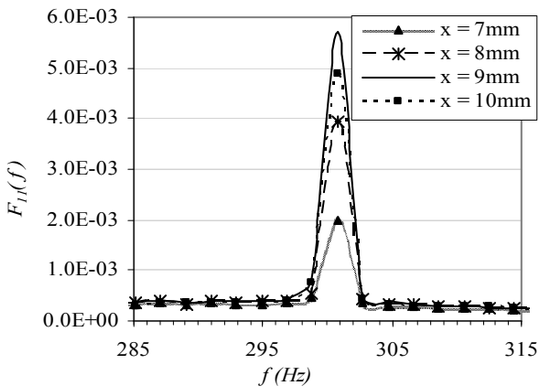

Fig. 6b: Evolution of the peak in the longitudinal power spectrum. Disturbance frequency 300Hz (approx.) $y^+ = 9$.

Figure 6b shows spectra for the same disturbance frequency taken at a fixed distance from the wall (0.52mm, $y^+ = 9$). Again the spike is clearly visible and it is seen to grow and then decay as the downstream coordinate increases from 7mm to 10mm

($x^+ = 122$ to $x^+ = 174$). It is noteworthy that it is only the amplitude that changes, while the width of the spike remains constant as expected.

This behavior must be contrasted with the evolution of a spectrally local disturbance in isotropic turbulence studied experimentally by Kellogg & Corrsin (1980) and numerically by Orlandi & Crocco (1985). In both those studies the spike rapidly decayed accompanied by spreading of the width.

4. KLEBANOFF MODES

4.1 Elucidating the vorticity source

Both Fasel (2002) and ourselves have been using vorticity sources derived from fictitious body forces to generate streaklike structures. Hitherto, however, we had little idea what form the vortical structures generated by these forces took. Considering, first, the simple case of a uniform flow, with this approach the governing equation for streamwise vorticity takes the form:

$$\frac{D\omega_x}{Dt} = Gg(y - y_S)\delta(x - x_S)F(t)\cos\beta z + \nu\nabla^2\omega_x \qquad (4)$$

where the LHS term is the material derivative; (x,y,z) are, respectively, the streamwise, wall-normal and spanwise coordinates; G is a constant source strength ; (x_s, y_s) are the source coordinates; δ is a delta function; g = δ in our work but Fasel uses g = dδ/dy; F(t) = H(t) – H(t_f) where H is the Heaviside step function; and ν is kinematic viscosity. If viscous effects are neglected the solution is

$$\begin{aligned} \omega_x &= Gg(y - y_S)H(x - x_S)F(t)\cos\beta z \\ \omega_z &= 0 \end{aligned} \qquad (5)$$

Thus we can see that in our case of a δ function source a simple vorticity sheet is generated which has alternating sign of vorticity in the spanwise direction. Fasel's source produces a somewhat more complex (double-δ vorticity sheet). In the case of the laminar boundary layer when the source is placed just above the edge of the boundary layer, the vortex sheet models the zero- and low-frequency streamwise vortical structures in the free stream. Kudar (2006), Kudar et al. (2005,2006) have shown that the laminar boundary layer is only receptive to very low-frequency streamwise vorticity and not at all to freestream spanwise vorticity.

When such a vorticity source is inserted in to a turbulent boundary layer (Ali & Carpenter 2005), the structures it generates model the hairpin vortices seen in the near-wall region. It is these that generate the sublayer streaks.

It is evident from eq. (5) that a very strong narrow shear layer will form around y = y_s, so we cannot really neglect viscous effects. We can drop $\partial^2\omega_x/\partial x^2$ on the RHS of eq. (4) because it is higher order. For x >> x_s a quasi-self-similar steady state solution can be found that takes the form:

$$\omega_x = \frac{\hat{\Omega}(\eta)}{2\nu(x - x_S)}; \qquad \eta = \frac{y - y_S}{\sqrt{2\nu x}} \qquad (6)$$

This follows from the identity

$$\delta(y - y_S) = \exp(-\eta^2/2)/\sqrt{2\pi\nu x} \quad \text{as } \nu x \to 0.$$

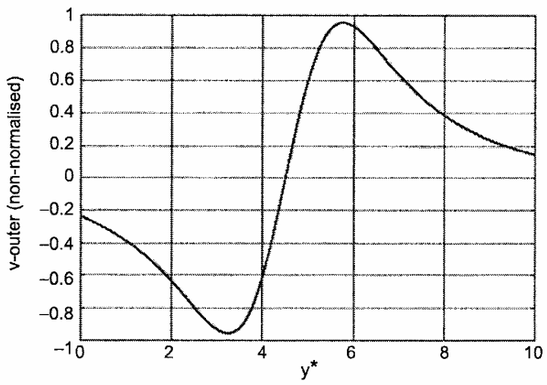

Fig. 7: Un-normalised wall-normal velocity profile created in uniform flow by Fasel (2002) double-δ vorticity source.

The Poisson relation between vorticity and stream function, namely

$$\frac{\partial^2\psi}{\partial z^2} + \frac{\partial^2\psi}{\partial y^2} = -\omega_x \qquad (7)$$

is then combined with eqs. (4) and (6) to derive a fourth-order ODE for ψ that is solved numerically to give the velocity field. Fig. 7 shows the (un-normalized) wall-normal velocity profile for the Fasel source.

Essentially the boundary-layer is driven by the wall-normal and spanwise velocity field of the streamwise vortex sheet created by the vorticity source. A corresponding quasi-similar solution can be derived within the boundary conditions at the wall; this is also required to match the uniform-flow solution. The composite wall-normal and streamwise velocity profiles are depicted in Fig 8 and 9 respectively. These composite solutions agree well with the numerical-simulation results given in Fasel (2002).

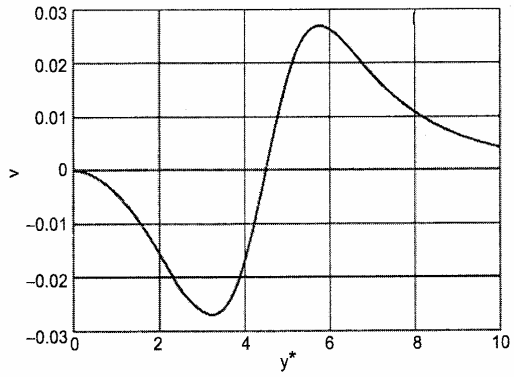

Fig. 8: Composite wall-normal velocity profile corresponding to Fasel (2002)

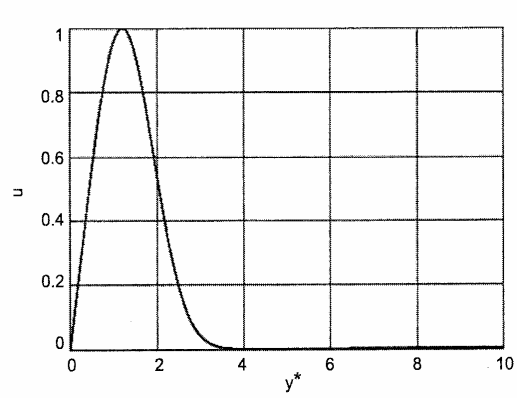

Fig. 9: Composite wall streamwise velocity profile corresponding to Fasel (2002)

4.2 Non-linear interaction between Klebanoff modes and 2D TS waves in laminar boundary layer:

Let the flow perturbation variables be written as:

$$\phi = (u,v,w,p) \tag{8}$$

then we consider a scenario whereby

$$\phi = \phi_1 + \phi_2 + \phi_3 \tag{9}$$

where,

$$\phi_1 = \{\hat{u}_1(y), \hat{v}_1(y), \hat{p}_1(y)\}\cos\beta z; \quad \hat{w}_1(y)\sin\beta z \tag{10}$$

corresponds to the Klebanoff mode whose solution was described above;

$$\phi_2 = \{\hat{u}_2(y), \hat{v}_2(y), \hat{p}_2(y)\}e^{i(\alpha_2 x - \omega t)}; \quad \hat{w}_2 = 0 \tag{11}$$

corresponds to the 2D TS wave which we will also regard as known; and

$$\phi_3 = \{\hat{u}_3(y)\cos\beta z, \hat{v}_3(y)\cos\beta z, \hat{w}_3(y)\sin\beta z, \hat{p}_3(y)\cos\beta z\}\exp[i(\alpha_3 x - \omega t] \tag{12}$$

corresponds to the oblique waves generated by the nonlinear interaction between ϕ_1 and ϕ_2.

The governing equation for $\hat{v}_3$ can be derived from the Navier-Stokes equations and takes the form:

$$L_{os}(\alpha_3)v_3 = R_f e^{i(\alpha_2 - \alpha_3)x} \tag{13}$$

where L_{os} is the Orr-Sommerfeld operator and the forcing term

$$R_f = [-\alpha_3\alpha_2(u_1'u_2 + u_1u_2') + i\alpha_3(u_1'v_2' + u_1''v_2) + i\alpha_2\gamma^2 u_1 v_2]e^{i(\alpha_2-\alpha_3)x}; \quad \gamma^2 = \alpha_3^2 + \beta^2 \tag{14}$$

The solution to eq. (13) consists of the complementary function, $\tilde{v}_3$ (the solution or eigen function of the homogeneous equation) plus a particular solution of the form

$$\hat{v}_{total} = x\tilde{v}_3\bar{\lambda}e^{i(\alpha_2-\alpha_3)x} + v_{3f} \tag{15}$$

where the first term is the secular term and the second the non-secular forced solution. Eq.(13) can now be written as

$$L_3(\alpha_3)v_{3f} + \bar{\lambda}e^{i(\alpha_2-\alpha_3)x}L_2(\alpha_2)\hat{v}_3 = R_f \tag{16}$$

where L_2 is an operator the form of which follows from the governing equation. Using the theory of adjoints as in Sen et al. (2002,2006) the solvability condition gives

$$\bar{\lambda} = \int_0^\infty \theta_3 R_f dy \Big/ \int_0^\infty \theta_3 L_2(\alpha_3)\tilde{v}_3 dy \tag{17}$$

where θ_3 is the adjoint eigenfunction. Since R_f varies as the amplitude of the streak, $\bar{\lambda}$ is proportional to the streak strength. For weak streaks, i.e. $\bar{\lambda} << 1$, this only results in a correction to the eigen value of the form

$$\Delta\alpha_3 = -i\bar{\lambda}e^{i(\alpha_2-\alpha_3)x} \tag{18}$$

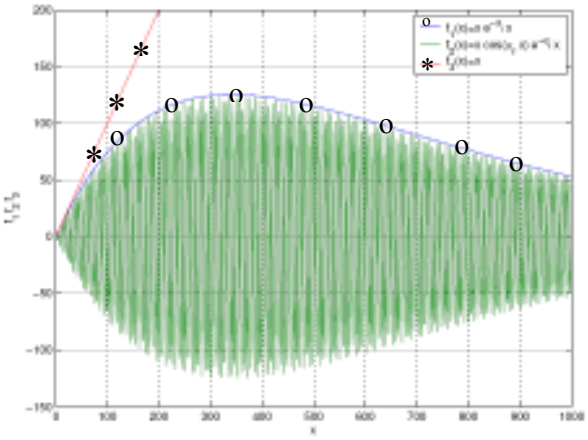

Fig. 10: Algebraic growth due to K (streaks) +2D TS +3D TS waves interacting for laminar damped case.

The difference in the real parts of the wave-numbers contributes a change of phase while the difference in imaginary parts leads to amplification or attenuation depending on its sign. This means that while propagating along the boundary layer $\Delta\alpha_3$ varies in magnitude owing both to phase and amplitude change. Hence, the effect is amplifying over short distances giving the intermittent bursting observed by Fasel (2002) in his simulations.

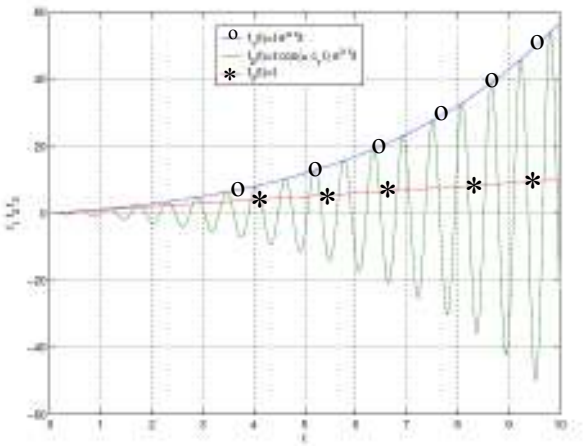

Fig. 11: Preliminary results for algebraic growth due to K (streaks+2D TS+3D TS waves interacting for turbulent

For stronger streaks leading to large $\overline{\lambda}$ the behaviour is qualitatively different because explosive algebraic growth can exist owing to the existence of the secular solution. We have demonstrated numerically that both scenarios are plausible and would expect algebraic growth to start to dominate when $u_1 \geq 0.1\ U_\infty$.

A typical result for algebraic growth for a laminar damped case is given in Figure 10. The spatial problem has been solved for a laminar boundary layer with the following input data (normalised by the free-stream velocity and boundary-layer thickness): R = 1500, ω = 0.4, β = 0.2. For this input we obtain eigenvalues α_2 and α_3 as:
α_2 = 0.48729 + *i* 0.002936 and α_3 = 0.98256 + *i* 0.00441142.

Corresponding to this $|\overline{\lambda}|$ = 0.15682, Figure 10 shows algebraic growth corresponding to the above parameters, plotted to a free scale for the vertical co-ordinate y. Also the x co-ordinate gives distance in x from the point of inception of algebraic growth. The function $f_1(x) = x\,e^{-\alpha_{ix}}$ is the envelope of the algebraic growth curve $f_2(x) = x\cos(\alpha_r x)e^{-\alpha_{ix}}$. Figure 10 shows the full function with the spatial variation in x for the parameters above. Also $f_3(x) = x$ shows the linear growth line corresponding to algebraic growth. It is seen that considerable algebraic growth occurs even though the mode is damped.

Figure 11 shows algebraic growth for an amplified turbulent mode with R = 5000, α = 31.0 and β = 17.90 using the boundary-layer thickness and freestream velocity as length and velocity scales respectively. This problem is investigated for algebraic growth in the temporal domain. The eigenvalues for the phase speeds c_2 and c_3, respectively for the 2D-TS and 3D-TS modes are given as:
c_2 = 0.350975 + *i* 0.00559564, c_3 = 0.300454 + *i* 0.00536667. All the corresponding values in inner variables (superscripted by a (+) sign) are given as follows.
$R^+ = 1$, $\alpha^+ = 0.1088$, $\beta^+ = 0.062832$,
$c_2^+ = 6.1581 + i\,0.98180$; $c_3^+ = 5.2717 + i\ 0.09417$.
$|\overline{\lambda}|$ corresponding to this mode is 15.1838.

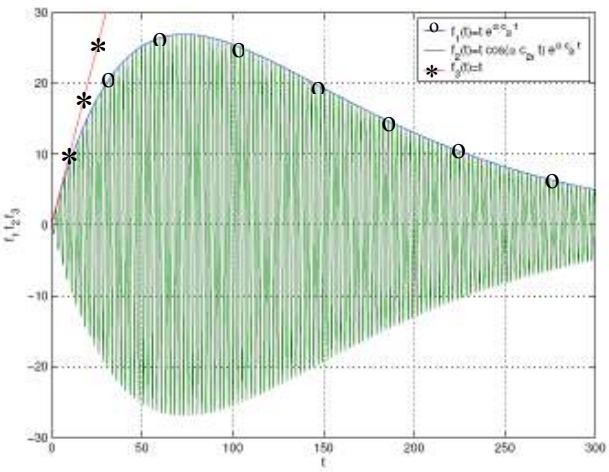

Fig. 12: Preliminary results for algebraic growth due to K (streaks+2D TS+3D TS waves interacting for turbulent damped case.

The growth rate αc_{2i} is given as 0.173464t. Since $c_{2i} > 0$, this mode is amplifying. Figure 10 shows plots again for $f_1(t) = t\,e^{\alpha c_{it}}$, $f_2(t) = t\cos(\alpha c_r t)\,e^{\alpha c_{it}}$

and $f_3(t) = t$ similarly as in figure 9, but this time for the temporal domain t. Clearly this figure shows algebraic growth, which is later superseded by exponential growth.

The next case is for a turbulent damped mode with R = 5000, $\alpha = 8.985$, $\beta = 17.90$**.** The eigenvalues for a phase speeds c_2 and c_3, respectively for the 2D-TS and 3D-TS modes are given as:

$c_2 = 0.282756 - i\ 0.00152036$, $c_3 = 0.187251 - i\ 0.01185049$. All the corresponding values in inner variables are given as follows:

$R^+ = 1$; $\alpha^+ = 0.03153$; $\beta^+ = 0.062832$; $c_2^+ = 4.9611 - i\ 0.026676$;

$c_3^+ = 3.2854 - i\ 0.208531$. $|\bar{\lambda}|$ corresponding to this mode is 2.6808. In this case the mode is damped and the growth rate is given as $\alpha c_{2i} = - 0.0136572$ t.

Figure 12 shows considerable algebraic growth before damping takes place.

Thus we see that both scenarios—the intermittent bursting observed by Fasel (2002) and the explosive algebraic growth described above— are possible. In both cases there is a low-frequency modulation with a period of approximately $36\nu/U_\tau^2$ corresponding to the bursting cycle. It is very close to the value of 36.6 measured by Klewicki *et al.* (1995) and of the same order of magnitude as the value of 80.5 found by Rao *et al.* (1971) and the value of 72 measured by Kline *et al.* (1967). Kim and Spalart (1987)obtained a value of 60 in their direct numerical simulations. Our preliminary analysis also shows that for a strong interaction between oblique waves and plane waves we need a spanwise wavelength of approximately 100 wall units. This agrees remarkably well with the streak spacing observed experimentally. Finally, the angle of propagation for the oblique waves in our theoretical model is approximately 60^o, close to that observed by Sirovich *et al.* (1990, 1991).

5. CONCLUSIONS

Fairly strong experimental evidence has been presented here for the theory outlined in S&V1 and S&V2. The shape of the eigenmode, obtained experimentally, matches the calculated eigenmode well. In the region of growth of the inner maximum the experimentally observed wave number, wave speed, growth rate etc. are in good agreement with the theoretical values. Thus we can claim that linear stability does provide a vital clue to the mechanism of sustenance of turbulence even in wall-bounded flows.

We have obtained a quasi-similar solution to the vorticity and stream function equations, in the presence of a free-stream body force, which reproduces the DNS results of Fasel (2002) almost exactly. It has been shown further that the triadic interaction between the K-modes and 2D- TS and 3D-TS waves could lead to explosive algebraic growth. This is most likely the mechanism of bypass transition. A similar mechanism could exist in fully developed turbulent wall flows wherein streamwise vortices in the near-wall region take the place of the free-stream body force used in the laminar flow calculations. The resulting K-modes and their interaction with 2D-TS and 3D-TS modes would lead to similar explosive growth (bursting), for which preliminary results have already been obtained. Thus interfering with generation of the unstable 2D-TS waves, say by using compliant surfaces (see Sen and Arora (1988)), would quench this mechanism and help in the control of turbulence in wall-bounded flows.

6. REFERENCES

1. Ali R. and Carpenter P.W., 2005, Effect of wall Compliance on Streak-like Flow structures, *Proc. 2nd Int. Symp. on Sea-water Drag Reduction*, Busan, Korea.
2. Carpenter P.W. and Garrad A.D., 1985, The hydrodynamic stability of flow over Kramer-type compliant surfaces Part 1. Tollmein-Schlichting instabilities, *J. Fluid Mech*., 150, 465-510.
3. Fasel H., 2002, Numerical investigation of the interaction of the Klebanoff-mode with a Tollmein-Schlichting wave, *J. Fluid Mech.*, 450, 1-33.
4. Hussain A.K.M.F. and Reynolds W.C., 1972, The mechanics of an organized wave in turbulent shear flow Part 2. Experimental results, *J. Fluid Mech.,* 54, 241-261.
5. Hussain A.K.M.F. and Reynolds W.C., 1975, Measurements in fully developed turbulent channel flow, *J. Fluids Eng*., 97, 568-578.
6. Josan P.S., 2004, Suppression of wall turbulence using a compliant surface based on stability and turbulence analysis, *Ph.D. Thesis*, IIT Delhi.
7. Kellogg R. M. and Corrsin S., 1980, Evolution of a spectrally local disturbance in grid-generated, nearly isotropic turbulence, *J. Fluid Mech.*, 96, 4, 641-669.
8. Kim, J. & Spalart, P.R. 1987 Scaling of the bursting frequency in turbulent boundarylayers at low Reynolds-numbers. *Phys. Fluids* 30, 3326-3328.
9. Klewicki, J.C., Metzger, M.M., Kelner, E. & Thurlow, E.M. 1995 Viscous sublayer flow visualizations at $R_\theta \approx$ 1500000. *Phys. Fluids* **7**, 857-863.
10. Kline, S.J., Reynolds, W.C., Schraub, F.A. & Runstadler, P.W. 1967 The structure of turbulent boundary layers. *J. Fluid Mech.* 30, 741-773.
11. Kudar K., Carpenter P.W. and Davies C., 2006, Klebanoff modes in swept boundary layers, In Govindarajan R. ed. *Sixth IUTAM Symposium on Laminar-Turbulent Transition,* Springer, 167-172.
12. Orlandi P. and Crocco L., 1985, Symposium on Turbulent Shear Flows, *5th, Ithaca, NY,*

August 7-9, 1985, Proceedings (A86-30201 13-34), 15.1-15.5.

13. Rao, K.N, Narasimha, R., & Narayanan, M.A.B. 1971 The `bursting' phenomenon in a turbulent boundary layer. J. Fluid Mech. 48, 339-352.
14. Reynolds W.C. and Hussain A.K.M.F., 1972, The mechanics of an organized wave in turbulent shear flow Part 3. Theoretical models and comparison with experiments, *J. Fluid Mech*., 54, 263-288.
15. Sen P.K. and Arora D.S., 1988, On the stability of laminar boundary layer over a flat plate with a compliant surface, *J. Fluid Mec*h*.,* 197, 201-240.
16. Sen P.K., Josan P.S. and Veeravalli S.V*.,* 2006, Suppression of wall turbulence based on stability and turbulence analysis using a compliant surface, In Govindarajan R ed. *Sixth IUTAM Symposium on Laminar-Turbulent Transition,* Springer., 231-236.
17. Sen P.K. and Veeravalli S.V., 1998, On the behaviour of organized disturbances in a turbulent boundary layer, *Sadhana*, 23, 167-193.
18. Sen P.K. and Veeravalli S.V., 2000a, Behaviour of organized disturbances in fully developed turbulent channel flow, *Sadhana*, 25, 423-437.
19. Sen P.K. and Veeravalli S.V., 2000b, Hydrodynamic stability theory and wall turbulence, *Current Science* 79 No.6 840-848.
20. Sen P.K., Hegde S. and Carpenter P.W., 2002, Simulation of small disturbance waves over alternate rigid and compliant panels, *Indian Journal of Engineering and Material Sciences*, 9 (6), 409-413.
21. Sirovich, L., Ball, K.S. & Keefe, L.R. 1990 Plane waves and structures in turbulent channel flow. *Phys. Fluids* A2, 2217-2226.
22. Sirovich, L., Ball, K.S. & Handler, L.R. 1991 Plane structures in wall-bounded turbulent fows. *Theor. Comput. Fluid Dynam*.2, 307-317.